Imaging of Avalanches in Granular Materials

Michael Bretz, Jevne B. Cunningham, Peter L. Kurczynski, and Franco Nori
Department of Physics, University of Michigan, Ann Arbor, Michigan 48109-1120
(Received 29 June 1992)

Dry, noncohesive granular materials were very slowly driven to the threshold of instability where they produced avalanches. We have used digital image analysis to record avalanches that occurred on the surface of the incline. Results show large slides every 10–13 min which reset the surface from the maximum angle of stability, θ_c, back to the angle of repose, θ_r. We also find a power-law distribution of sizes for smaller avalanches occurring *between* the large sliding events. The number of these small avalanches follows a power-law dependence on the reduced angle, $(\theta_c-\theta)/(\theta_c-\theta_r)$, or time, which demonstrates that θ_c behaves like a critical point.

PACS numbers: 81.35.+k, 64.60.Ht

The mechanical properties of granular materials are a subject of enormous interest to many disciplines [1], such as the mineral processing and chemical industries, and also to structural and civil engineers. Although physical chemists and physicists have studied powder mechanics, including cohesive and frictional forces, for over two centuries [2], most of this effort has focused on the two extreme steady states: the continuous flow and the static compact state. The intermediate or quasistatic regime of intermittent avalanches has been at the heart of much recent work, including several pretty experiments [3–7] and novel theoretical proposals (see, e.g., Refs. [8–12]). There has also been a recent renewed interest in other aspects of the physics of sand [13].

The properties of granular packings (e.g., segregation, arching, bistability, dilatancy) make these systems very difficult to study, creating substantial hysteresis and instabilities. This might explain why several experiments on granular systems have so far given somewhat mixed results regarding the criticality of the attractor, or self-organized state. For instance, some experiments [3] report avalanches that occur with a mean size and lifetime, while the study of small conical piles growing by the addition of individual grains [6] shows a power-law distribution of events for small piles, and relaxation oscillations for larger piles. Both of these experiments measured only the flow past the rim of the sandpile, and they did not record events which occurred totally within the pile. Rosendahl and Rutledge [7] did examine the events occurring between successive large slides on conical piles and found many small avalanches with an approximate power-law distribution of sizes. We stress that the conical pile configuration is very different from incline ramping experiments. It is the purpose of this work to study the transition between static and flowing states in very slowly driven granular assemblies using digital imaging to record and analyze individual avalanches.

Our experiment consisted of slowly rotating a high-walled Plexiglas tray containing molecular sieve spheres of about 2 mm diameter (grade 514GT, 4 Å). This granular material was chosen for its water absorptive property which ensured that cohesive forces remained negligible. The bottom of the tray was prepared by gluing down a variable number of layers of grains to give a rough surface profile of 4–5 mm. The tray was filled to a 5 cm depth and rotated about one end by means of a geared-down synchronous motor (1 rpm) attached to an external gear box and then to a bicycle gear assembly (see Fig. 1). The rotation speed was 0.22 deg/min, slower than that used in previous avalanche experiments. The tray was initially set at a 20° tilt and the granules raked to the angle of repose. As the tray rotated, we observed a series of large slides involving most or all of the upper grain layers. These slides effectively "reset" the bed to the angle of repose and smoothed out the surface. The run was halted when the bare substrate just began to appear at the top of the tray. The presence of the rough substrate is especially important, because without it the granular bed slid frequently over the slick bottom surface of the tray. With the substrate layer to provide friction, however, a much richer behavior was observed.

Any two consecutive large slides were separated by a

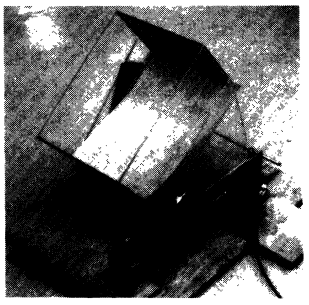

FIG. 1. The rotating tray apparatus used in our experiment. The aggregate was confined to an open-top rectangular box ($19\frac{1}{2}$ in. $\times 14\frac{3}{8}$ in. $\times 11\frac{1}{2}$ in.) made of clear and amber $\frac{1}{4}$-in. Lucite sheeting. The tray was rotated about a fixed axis by a four-gear bicycle drive train powered by a 1-rpm synchronous motor through a set of smaller gears. The tray has an ascension rate of 0.22 deg/min and is felt-dampened to absorb vibrations during motion.

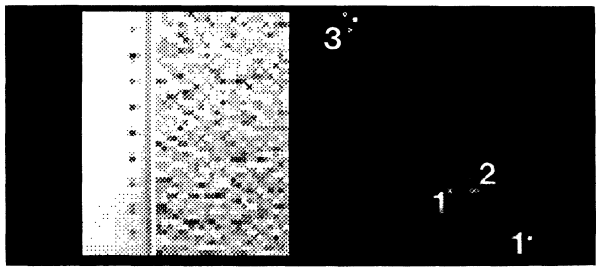

FIG. 2. A cropped, subtracted image as seen by the CCD camera monitoring the avalanches: The brightest pixels correspond to very small avalanches of m grains, as indicated. Inset: A digital snapshot of a fraction of the surface of the granular assembly. The resolution is about 2 mm/pixel as indicated by a ruler with (unresolved) cm marks on it (equivalent to about 1 pixel per grain of material).

sequence of small avalanches which were recorded with a charge-coupled-device (CCD) camera (EDC-1000, Electrim Corp.) interfaced to a computer and controlled with an associated image processing software (IPS-Edit, F. J. Phillips). The 192×165 pixel array camera was mounted from the ceiling 2 m above the particle tray. The field of view was approximately perpendicular to the avalanching surface and covered about $\frac{3}{4}$ of the bed, leaving an inch to the left, right, and lower tray walls. This alignment tended to minimize boundary effects and maximize observation time before layer thinning occurred at the top of the viewing field. Diffuse lighting was supplied with twin fluorescent lamps, covered with tracing paper and positioned 0.5 m in front of the tray.

The camera updated images once per second but the computer was instructed to record pictures only when it detected a change in the field of view, a feature ideal for recording avalanches. Successive images were later digitally subtracted by a C^{++} program to retain only the avalanche information, and then counted, stored, and analyzed to obtain the size distributions and other quantities. (See Fig. 2 for details. Date and time stamping occupied the bottom nine pixels of each photograph.)

Avalanche sizes and positions were determined sequentially by a raster scan of pixels in the subtracted image. When a pixel of absolute brightness above a predetermined threshold value was detected, an avalanche size (pixel counting) routine was entered. Here, surrounding pixels were compared to the threshold. If they too were above it, then the program would continue to count pixels in the immediate neighborhood by following a U-shaped pattern that grew down and out in size with each iteration. The routine stopped if three passes at successively larger radii did not yield any pixels above the threshold. A data file was produced containing the x-y coordinates of the starting pixel (upper left corner) of the avalanche, the size in pixels, and other information, such as average light intensity and time. The routine then reset all pixels found to zero intensity (to avoid recounting) and continued the raster scan search for further avalanches.

In order to test the reliability of the avalanche counting routine, a large number of pictures were visually compared with the text output file. The reliability of this algorithm was verified for avalanches up to about 20 bright pixels in size. Larger avalanches, however, required a visual size determination. Scanning was also necessary to screen for the double counting of avalanches which occasionally appeared on consecutive pictures. The pixel cutoff threshold was chosen to be appropriate for counting the avalanching final grain positions while neglecting the less intense pixels of the grain starting positions.

We observed 4 or 5 large sliding events in each data series during which the overall slope of the bed oscillated between $\theta_r \simeq 25°$ and $\theta_c \simeq 28°$. Figure 3(a) shows the cumulative (i.e., integrated) number of avalanches N versus time for a typical run. Vertical risers correspond to the number of avalanches occurring within a single picture. Horizontal lines correspond to a period of no avalanches [which can be for up to 2 min just after a slide; see, for instance, the lower left corner of Fig. 3(a)]. In addition to large slides at the start and end of the Fig. 3(a) data set, arrows represent times within the data set at which large slides occurred [but whose contributions to N are not included in Fig. 3(a)].

Here we will focus on the very rich behavior of the "precursor" small avalanches leading up to a large slide. The data between the arrows are analyzed in Fig. 3(b), where N and also A, the avalanche area, are both plotted versus reduced time, $t=(T_c-T)/(T_c-T_r)$, or equivalently the reduced angle, $\phi=(\theta_c-\theta)/(\theta_c-\theta_r)$. The repose time T_r occurs at the end of a slide and the critical time T_c is taken as the start of the next slide (slides are 3–4 sec long). The repose angle θ_r was measured and θ_c was then calibrated from the ramp speed and T_c-T_r. Far from the critical angle, N grows slowly. At $t\sim 0.12$ [dotted arrow in Fig. 3(a)] the computer picture reveals a subtle below-threshold avalanche activity of the lower half of the field of view as the grains collectively reposition themselves. This slight downhill shift is an adjustment of the top layer of grains within their respective local potential wells. For a decade at smaller t, N grows logarithmically until the bed eventually slides at T_c. The line in Fig. 3(b) is a best logarithmic fit to this part of the data set. It is important to mention that a logarithmic divergence also occurred in runs using a faster (4 rpm) motor. The cumulative avalanche area A roughly follows the same logarithmic behavior. The technical difficulties associated with the size determination of the largest avalanches adds noise to these results. For $t \lesssim 10^{-2}$ the N and A data in Fig. 3(b) round off, even though the limit of the computer image update time is not reached until $t \lesssim 1.5\times 10^{-3}$. We believe that a finite-size effect (tray walls or the rough substrate) is limiting the logarithmic growth.

Since the integrated number of avalanches $N(t)$ behaves like $N(t)=\int_{T_r}^{t} n(t')dt' \propto \log(t)$, the number of

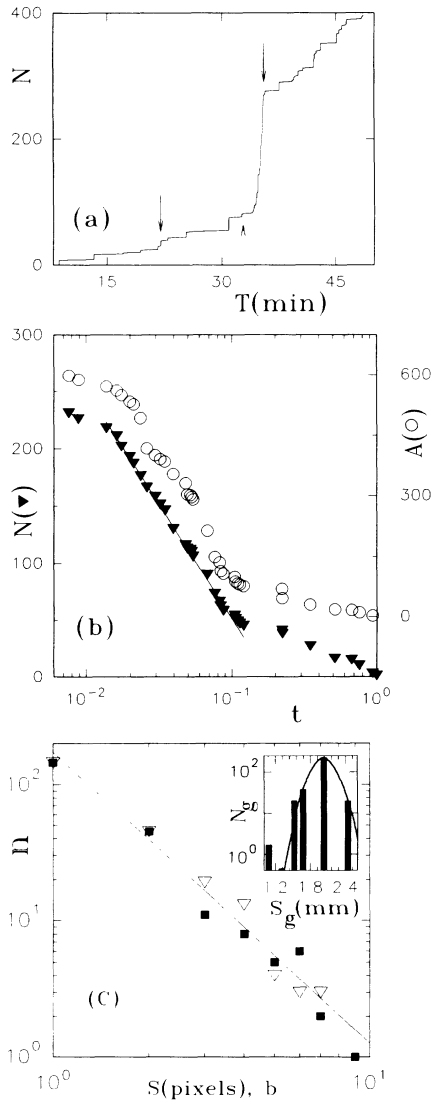

FIG. 3. (a) Cumulative (i.e., integrated) number of avalanches N vs time for one run. The data between two large slides (indicated by solid arrows) is analyzed in (b), where N (▼) and also A (○), the cumulative avalanche area, are both plotted vs reduced time t or equivalently the reduced angle ϕ. The line is a best logarithmic fit to the N data over the region after the dotted arrow in (a). (c) Number of avalanches n (■) vs size s (in pixels) for the data shown in (b). A linear fit to the data gives $n(s) \sim s^{-2.134}$. For comparison purposes, we also show the same data binned in powers of 2 (▽), where $s = 2^{b-1}$ and b corresponds to the bin number. Inset to (c): Distribution N_g of grain sizes S_g as determined by counting the fraction of grains which are caught by a series of standard meshes. A Gaussian distribution with a mean of 2.02 mm and a standard deviation of 0.19 mm is shown as the solid line.

avalanches $n(t)$ has a *power-law behavior over time* with an exponent of -1, i.e., $n(T) \propto 1/(T_c - T)$ for small t. Further analysis shows that the number of avalanches n plotted versus size s (number of pixels above threshold)

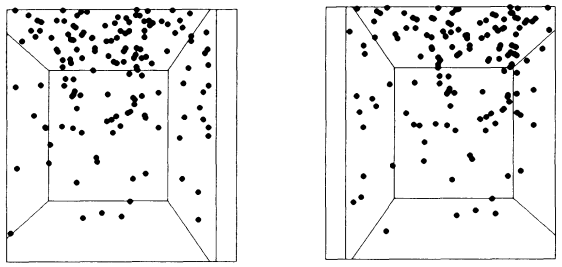

FIG. 4. Stereo view of the location (x_0, y_0, t) of the avalanche starting point (defined here as the leftmost top of an avalanche) for the avalanches in Fig. 3(b). Depth increases with time in the picture of size 192×158 pixels. The viewing box superimposed on the pictures has an inverse perspective.

exhibits the power-law dependence $n(s) \sim s^{-2.134}$ [see Fig. 3(c)]. For comparison purposes, we also present the same data binned in powers of 2, where $s = 2^{b-1}$, b corresponds to the bin number, and with the independent variable s ranging from 1 to 512, or over 2.5 decades. In this power-law binning, each point corresponds to the number of avalanches between successive powers of 2. Regardless of the binning used, a power law fits our data. Moreover, $n(s)$ exhibits a power-law behavior for the whole run, i.e., not only for the data (between the solid arrows) preceding a slide.

The results presented in Figs. 3(b) and 3(c) indicate that the dynamical process of slowly tilting an originally flat granular bed evolves the system to a state (the attractor) where transport takes place through events on several time and length scales, i.e., our system is slowly driven to a critical state. Of course, more work is needed in order to appreciably extend power-law behavior over more than the decade that we observed; however, our observations and conclusions, obtained by looking at two different physical quantities and using different ramping rates, are compelling because of their mutual consistency.

In traditional critical phenomena, critical exponents describe equilibrium static properties, while here they describe nonequilibrium dynamical properties. If the slope θ of the system is forced beyond θ_c, there will be a continuous spontaneous flow j. This particle flow or current is the analog of the magnetization or order parameter [8]. The deviation from the critical slope plays the role of the reduced temperature. The analog of the magnetic field is either the current of incoming particles, for a conical pile configuration [6], or the rate of slope increase, for our system.

We have obtained scatter plots of the position of each avalanche in our field of view (depth increases with time). Figure 4 shows a stereo view of the location (x_0, y_0, t) of the avalanche origin (or starting point, defined here as the leftmost top of an avalanche) for the avalanches used for the logarithmic fit of Fig. 3(b). The top of the field of view shows a stronger concentration of avalanches, most likely because particles towards the top of the tray are

packed less densely than those closer to the bottom. Thus, particles there have a greater range of freedom. The much higher density of points at depths close to the large rectangle in the stereo graphs reflects the much higher number of avalanches at times close to T_c. The majority of very small avalanches, which occur in the upper half of the tray, *do not reach the bottom rim.* We refer the reader to Jensen, Christensen, and Fogedby [9,10] for a lucid discussion on the differences in observed size distribution between the flow of sand (i) down the slope and (ii) over the rim of the sandpile.

Further work is needed to investigate the important effects of particle density. Close packing in high-density granular systems increases the region of bistable behavior. When driven above the angle of repose, avalanches in close-packed systems are infrequent at first since a large number of particles are constrained by neighboring grains. When avalanches in such systems occur, they are more likely to be global reorganizations (e.g., our observed shift in the bed for $t < 0.12$) instead of minor fluctuations. Therefore, a power-law response would not be expected. As the density is decreased, more small events should occur since the particles have more room between them to locally readjust their locations. In fact, it has been proposed that for granular systems to be in a self-organized critical state, the density must have a critical value [5].

Packing density could also be influenced by residual vibrations of the mechanical setup. Care was taken to provide a quiet, still environment during data taking since we observed that blowing gently or speaking directly into the tray at high grain bed angles sometimes triggered slides. We also took advantage of a timely sub-basement building survey to compare the floor and experimental platform vertical vibrations during daytime working hours (our avalanche data sets, however, were taken either at night or during weekends). A felt pad placed under the experiment damped floor vibrations adequately, although there did remain sharp spikes at frequencies between 25 and 58 Hz. However, these spikes contributed very little to the overall vibrational energy.

In summary, we used digital image analysis to record avalanches on the face of a granular bed. Results show large sliding events every 10–13 min in addition to smaller avalanches with a power-law distribution of sizes. The number of avalanches versus the reduced angle or time also shows a power-law dependence, which suggests that θ_c is analogous to the critical point of a higher-order phase transition.

We would like to acknowledge Joshua H. Bretz for his help with the computer system. This work was supported in part by the University of Michigan (UM) protein structure and design program and NSF Grant No. DMR-90-01502. J.B.C. and P. L. K. received support for undergraduate students from the UM and the NSF-REU.

[1] R. L. Brown and J. C. Richard, *Principles of Powder Mechanics* (Pergamon, New York, 1966); R. A. Bagnold, *The Physics of Blown Sand and Desert Dunes* (Methuen, London, 1941); S. B. Savage and K. Hutter, J. Fluid Mech. **176**, 67 (1989).

[2] C. A. Coulomb, Acad. R. Sci. Mem. Math. Phys. **7**, 343 (1773); O. Reynolds, Philos. Mag. **20**, 469 (1885).

[3] H. M. Jaeger, C.-H. Liu, and S. R. Nagel, Phys. Rev. Lett. **62**, 40 (1989).

[4] P. Evesque and J. Rajchenbach, C. R. Acad. Sci. Ser. 2 **307**, 223 (1988); in *Powders and Grains*, edited by J. Biarez and R. Gourves (Balkema, Rotterdam, 1989), p. 217.

[5] P. Evesque, Phys. Rev. A **43**, 2720 (1991).

[6] G. A. Held *et al.*, Phys. Rev. Lett. **65**, 1120 (1990).

[7] J. Rosendahl and J. E. Rutledge (unpublished).

[8] P. Bak, C. Tang, and K. Wiesenfeld, Phys. Rev. Lett. **59**, 381 (1987); C. Tang and P. Bak, *ibid.* **60**, 2347 (1988).

[9] H. J. Jensen, K. Christensen, and H. C. Fogedby, Phys. Rev. B **40**, 7425 (1989).

[10] H. J. Jensen, Phys. Rev. Lett. **64**, 3103 (1990).

[11] P. A. Thompson and G. S. Grest, Phys. Rev. Lett. **67**, 1751 (1991).

[12] O. Pla and F. Nori, Phys. Rev. Lett. **67**, 919 (1991).

[13] See, e.g., G. Baxter *et al.*, Phys. Rev. Lett. **62**, 2825 (1989); H. Caram and D. Hong, *ibid.* **67**, 828 (1991); P. Evesque and J. Rajchenbach, *ibid.* **62**, 44 (1989); C.-h. Liu, H. M. Jaeger, and S. R. Nagel, Phys. Rev. A **43**, 7091 (1991); H. M. Jaeger and S. R. Nagel, Science **255**, 1523 (1991), and references therein.

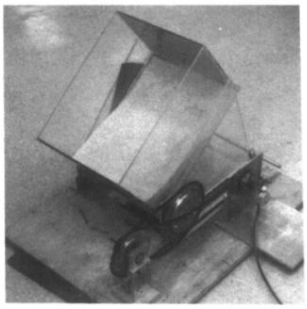

FIG. 1. The rotating tray apparatus used in our experiment. The aggregate was confined to an open-top rectangular box ($19\frac{1}{2}$ in.$\times 14\frac{3}{8}$ in.$\times 11\frac{1}{2}$ in.) made of clear and amber $\frac{1}{4}$-in. Lucite sheeting. The tray was rotated about a fixed axis by a four-gear bicycle drive train powered by a 1-rpm synchronous motor through a set of smaller gears. The tray has an ascension rate of 0.22 deg/min and is felt-dampened to absorb vibrations during motion.

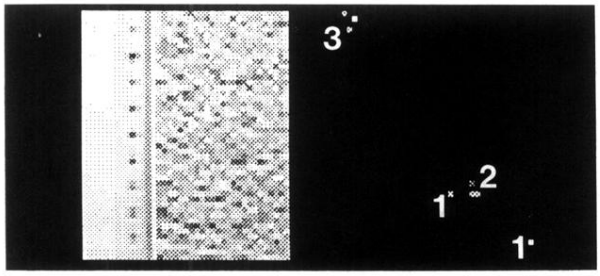

FIG. 2. A cropped, subtracted image as seen by the CCD camera monitoring the avalanches: The brightest pixels correspond to very small avalanches of m grains, as indicated. Inset: A digital snapshot of a fraction of the surface of the granular assembly. The resolution is about 2 mm/pixel as indicated by a ruler with (unresolved) cm marks on it (equivalent to about 1 pixel per grain of material).